J Membrane Biol (2015) 248:951–965
DOI 10.1007/s00232-015-9847-0

BRIEF COMMUNICATION

Synthesis, Molecular Structure, DNA/Protein Binding, Cytotoxicity, Apoptosis, Reactive Oxygen Species, and Mitochondrial Membrane Potential of Dibenzoxanthenes Derivatives

Hui-Hui Yang[1] · Bing-Jie Han[1] · Wei Li[1] · Yun-Jun Liu[1] · Xiu-Zhen Wang[1]

Received: 28 May 2015 / Accepted: 18 September 2015 / Published online: 23 September 2015

Abstract Two dibenzoxanthene isomers **3** and **4** were synthesized and characterized. The crystal structures of the two compounds were solved by single-crystal X-ray diffraction. Binding of two compounds with calf thymus DNA (CT DNA) and BSA (bovine serum albumin) has been thoroughly investigated by UV–Vis and fluorescence spectroscopy. The DNA-binding constants were determined to be 2.51 ($\pm$0.09) $\times$ 10^3 for compound **3** and 4.55 ($\pm$0.10) $\times$ 10^3 for compound **4**. Two compounds can cleave pBR322 DNA upon irradiation. Significant nuclear damages of BEL-7402 cells were observed with compound treatment in a comet assay. The cytotoxicity in vitro was investigated by MTT method. These compounds have been found to induce nuclear condensation and fragmentation in BEL-7402 cells. The two compounds can enhance intracellular reactive oxygen species and decrease the mitochondrial membrane potential. The compounds activated caspase-3 and caspase-7, down-regulated the expression levels of anti-apoptotic protein Bcl-2, and up-regulated the expression levels of pro-apoptotic protein Bax. These compounds induce apoptosis of BEL-7402 cells through an ROS-mediated mitochondrial dysfunction pathway.

Keywords Bibenzoxanthene · DNA binding · Comet assay · Cytotoxicity · Apoptosis

✉ Yun-Jun Liu
lyjche@163.com

✉ Xiu-Zhen Wang
wxzqq1234@163.com

[1] College of Pharmacy, Guangdong Pharmaceutical University, Guangzhou 510006, People's Republic of China

Introduction

DNA is a good target for anticancer and antibiotic drugs because it is the material of inheritance and controls the structure and function of cells (Kelly et al. 1985). The interactions of small molecules with DNA can cause DNA damage in cancer cells, blocking the division of cancer cells and resulting in cell death (Zuber et al. 1998; Hecht 2000). Like DNA, protein is also considered to be one of the prime molecular targets for diagnostic and imaging agents, and so equal attention has been paid on designing novel probes for proteins. Benzoxanthenes are an important class of biologically active heterocycles, which possess analgesic (Hafez et al. 2008), anti-inflammatory (Poupelin et al. 1978), antibacterial (Hideo and Teruomi 1981), and antiviral activities (Lambert et al. 1997). Because of their interesting spectroscopic properties, these compounds have been employed as dyes (Menchen et al. 2003), pH-sensitive fluorescent materials for visualization of biomolecules (Knight and Stephens 1989), and in laser technologies (Ahmad et al. 2002). In recent years, benzoxanthene derivatives have received extensive interest in pharmaceutical industry and are considered as high-priority structures in combinatorial drug discovery and development. Benzoxanthenes have also been utilized as antagonists for paralyzing action of zoxazolamine (Saint-Ruf et al. 1975) and in photodynamic therapy (Ion 1997). Due to their wide range of interesting biological and therapeutic properties, many compounds related to benzoxanthene have been reported (Knight and Little 2001; Jha and Beal 2004; Bekaert et al. 1992; Ohishi et al. 2001; Gong et al. 2009; Nandi et al. 2009). Based on our previous studies (Wang et al. 2012, 2013, 2014), in this article, we report two new dibenzoxathene isomers 2-ONEDDX **3** (2-ONEDDX = 1-oxo-2-(*N*-methyl-aminocarbonyl)-13c-methoxyl-1,13c-dihydroxyl-dibenzo[a,kl]xanthene) and 8-ONEDDX **4** (8-ONEDDX = 1-oxo-8-(*N*-methyl-

aminocarbonyl)-13c-methoxyl-1,13c-dihydroxyl-dibenzo[a,kl]-xanthene). They were prepared by domino reaction with binaphthols and $CuCl_2$–ethanolamine complex as a catalyst (Scheme 1). To explore the biological effect of these dibenzoxanthene isomers, we studied their DNA-binding behaviors through electronic absorption titration, viscosity measurements, fluorescence spectra, and photoactivated cleavage. Binding abilities of two compounds with BSA were determined using UV–visible and fluorescence methods. In addition, we investigated the cytotoxicity of the two compounds toward BEL-7402, HeLa, A549, and SK-BR-3 cell lines by MTT assay. The apoptosis of BEL-7402 cells induced by the compounds was studied. The intracellular reactive oxygen species and mitochondrial membrane potential were assayed by fluorescence microscope. The cellular uptake and western blot analysis were investigated.

Experimental Section

Materials and Methods

NMR spectra were recorded on a Varian spectrometer. All chemical shifts were given relative to tetramethylsilane (TMS). Electrospray mass spectra (ES-MS) were recorded on an LCQ system (Finnigan MAT, USA) using methanol as a mobile phase. Microanalysis was carried out with a Perkin-Elemer 240Q elemental analyzer. UV/Vis spectra were recorded on a Shimadzu UV-3101PC spectrophotometer at room temperature. TLC analysis was performed on glass-backed plates (Merck) coated with 0.2 mm silica $60F_{254}$.

Common reagent-grade chemicals are commercially available and were used without further purification. Binaphthol **1** was prepared according to literature procedure (Wang et al. 2005). Calf thymus DNA (CT DNA) was obtained from the Sino-American Biotechnology Company. Cell lines of BEL-7402 (hepatocellular), HeLa (human cervical cancer), A549 (lung cancer), and SK-BR-3 cells (human breast cancer) were purchased from American Type Culture Collection. Doubly distilled water was used to prepare buffers (5 mM Tris(hydroxymethylaminomethane)-HCl, 50 mM NaCl, pH 7.2). A solution of CT DNA in the buffer gave a ratio of UV absorbance at 260 and 280 nm of ca. 1.8–1.9:1, indicating that the DNA was sufficiently free of protein (Reichmann et al. 1954). The DNA concentration per nucleotide was determined by absorption spectroscopy using the molar absorption coefficient (6600 M^{-1} cm^{-1}) at 260 nm (Chaires et al. 1982).

Synthesis of Two Isomers

Synthesis of Compound 2

A mixture of binaphthol **1** (0.344 g, 1 mmol) and methylamine (0.045 g, 1.5 mmol) in 15 mL methanol was stirred for 2 h at room temperature to give yellow solution. The solvent was removed under reduced pressure, and the crude product was purified by column chromatography on silica gel (100–200 mesh) with a mixture of EtOAc-petroleum ether (1:2, v/v) as an eluent. Thus the yellow product was obtained. Yield, 82 %, ^{1}H NMR (500 MHz, Acetone-d_6) δ: 8.58 (s, 1H), 7.92–7.85 (m, 3H), 7.37–7.34 (d, $J = 9.0$ Hz, 1H), 7.32–7.28 (m, 4H), 7.26–7.06 (m, 2H), 3.01 (s, 3H). ESI–MS, *m/z*: 343 ([M]). Anal. calcd for $C_{22}H_{17}NO_3$: C, 76.95, H, 4.99, N, 4.08; found C, 76.84, H, 4.92, N, 4.10 %.

Synthesis of Compounds 3 and 4

To a stirred solution of $CuCl_2$ (0.350 g, 2 mmol) and ethanolamine (0.120 g, 2 mmol) in 15 mL MeOH, 3-(*N*-

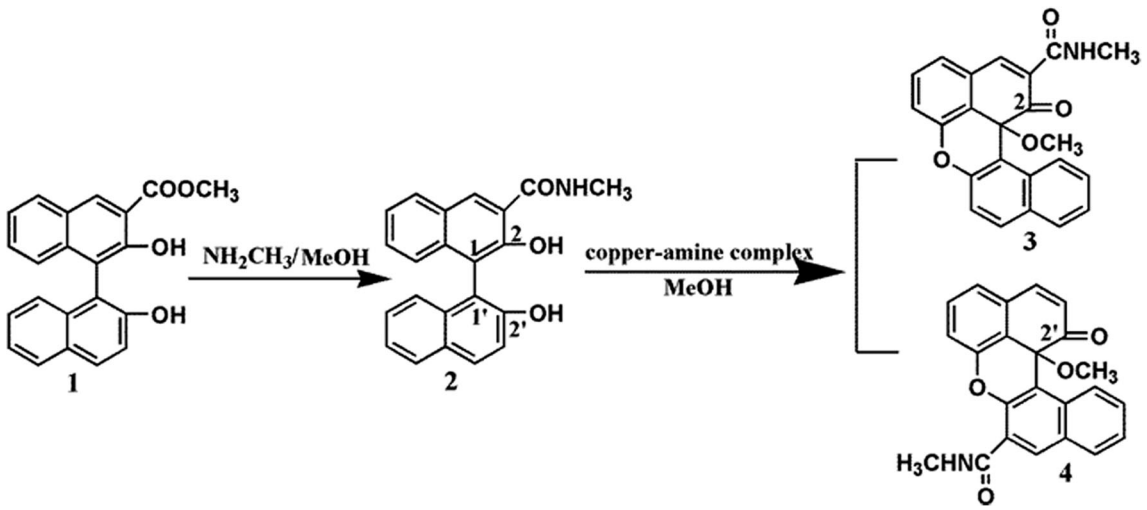

Scheme 1 The synthetic route of compounds **3** and **4**

methyl-aminocarbonyl)-binaphthol **2** (0.343 g, 1 mmol) was added at 50 °C. The mixture was stirred for 4 h, the reaction was quenched with 5 % $NH_3{\cdot}H_2O$, and the mixture was extracted with EtOAc. The organic extract was washed with water and dried over anhydrous Na_2SO_4. The solvent was evaporated and crude product was purified by column chromatography on a neutral alumina (EtOAc-petroleum ether, 1:2 v/v). The yellow powders of compounds **3** and **4** were obtained. Compound **3**: Yield, 30 %, ^{1}H NMR (500 MHz, DMSO-d_6) δ: 8.09 (d, $J = 9.0$ Hz, 1H), 8.00 (d, $J = 9.0$ Hz, 1H), 7.95 (d, $J = 10.0$ Hz, 1H), 7.58 (t, $J = 7.5$ Hz, 1H), 7.52–7.40 (m, 4H), 7.34 (d, $J = 8.0$ Hz, 1H), 7.27 (d, $J = 8.0$ Hz, 1H), 3.17 (s, 3H), 2.50 (s, 3H). ^{13}C NMR (125 MHz, DMSO-d_6) δ: 197.74, 162.38, 151.34, 151.13, 141.56, 132.39, 131.93, 131.70, 130.70, 130.63, 128.39, 127.19, 126.73, 126.39, 124.70, 117.74, 117.20, 116.35, 115.27, 106.58, 75.76, 51.07, 26.35. ESI–MS, *m*/*z*: 371 ([M]). Anal. calcd for $C_{23}H_{17}NO_4$: C, 74.38, H, 4.61, N, 3.77; found C, 74.45, H, 4.57, N, 3.68 %.

Compound **4**: Yield, 34 %, ^{1}H NMR (500 MHz, DMSO-d_6) δ: 8.20 (s, 1H), 8.00–7.98 (m, 1H), 7.96–7.93 (m, 1H), 7.52 (t, $J = 7.5$ Hz, 1H), 7.49–7.46 (m, 2H), 7.44 (d, $J = 10.0$ Hz, 1H), 7.31 (d, $J = 7.0$ Hz, 1H), 7.21 (d, $J = 7.5$ Hz, 1H), 6.33 (d, $J = 10.0$ Hz, 1H), 2.88 (s, 3H), 2.50 (s, 3H). ^{13}C NMR (125 MHz, DMSO-d_6) δ: 197.71, 165.56, 151.18, 147.83, 139.41, 132.89, 132.59, 131.55, 129.46, 128.72, 127.33, 126.64, 126.17, 126.28, 125.85, 125.11, 124.87, 116.67, 114.74, 107.77, 75.25, 51.25, 26.22. ESI–MS, *m*/*z*: 340 ([M-OCH_3]). Anal. calcd for $C_{23}H_{17}NO_4$: C 74.38, H, 4.61, N 3.77; found C, 74.48, H, 4.55, N, 3.80 %.

Crystal Structure Determination and Refinement of Compounds 3 and 4

Suitable single crystals of compounds **3** and **4** were mounted in glass capillaries for X-ray structural analysis. Diffraction measurements were performed with a Bruker Smart CCD area detector in the range $1.5° < \theta < 26°$ with Mo-Kα radiation ($\lambda = 0.71073$ Å) at 120 K. All empirical absorption corrections were applied using the SADABS program (Sheldrick 1996). The structures were determined using Patterson methods, which yielded the positions of all non-hydrogen atoms. All the hydrogen atoms of the compounds were placed in calculated positions with fixed isotropic thermal parameters, and the structure factor calculations were included in the final stage of full-matrix least-squares refinement. All calculations were performed using the SHELXTL-97 suite of the computer programs (Sheldrick 1997). The crystal data are shown in Table 1.

DNA-Binding Studies

The DNA-binding experiments were performed at room temperature. The absorption titrations of the compounds in buffer were performed using a fixed concentration (40 μM) for compounds to which increments of the DNA stock solution were added. Compound–DNA solutions were allowed to incubate for 5 min before the absorption spectra were recorded. The intrinsic binding constants *K*, based on the absorption titration, were measured by monitoring the changes in absorption at the aromatic band with increasing concentration of DNA using the following equation (Wolf et al. 1987):

$$[\mathrm{DNA}]/(\varepsilon_a - \varepsilon_f) = [DNA]/(\varepsilon_b - \varepsilon_f) + 1/K_b(\varepsilon_b - \varepsilon_f,) \quad (1)$$

where [DNA] is the concentration of DNA in base pairs and ε_a, ε_f, and ε_b correspond to the apparent absorption coefficient Aobsd/[compound], the extinction coefficient for the free compound, and the extinction coefficient for compound in the fully bound form, respectively. In plots of [DNA]/($\varepsilon_a - \varepsilon_f$) versus [DNA], K_b is given by the ratio of slope to the intercept.

Viscosity measurements were carried out using an Ubbelohde viscometer maintained at a constant temperature of 25.0 (±0.1) °C in a thermostatic bath. DNA samples approximately 200 base pairs in average length were prepared by sonication to minimize complexities arising from DNA flexibility. Flow time was measured with a digital stopwatch, each sample was measured three times, and an average flow time was calculated. Relative viscosities for DNA in the presence and absence of compounds were calculated from the relation $\eta = (t - t^0)/t^0$, where t is the observed flow time of the DNA-containing solution and t^0 is the flow time of buffer alone (Satyanarayana et al. 1993). Data were presented as $(\eta/\eta_0)^{1/3}$ versus binding ratio (Cohen and Eisenberg 1969), where η is the viscosity of DNA in the presence of compounds and η_0 is the viscosity of DNA alone.

Fluorescence Measurements

A 3.0 mL solution containing 40 μM of compounds was added to a 1.0 cm quartz cuvette and then titrated by successive addition of CT DNA solution. The solution was allowed to stand for 5 min to equilibrate, and the fluorescence spectra were recorded in the wavelength range of 400–650 nm with an exciting wavelength at 315 nm. The appropriate blanks corresponding to the Tris–HCl buffer solution were subtracted to correct the background of the fluorescence.

Table 1 Crystal data for compounds **3** and **4**

	Compound **3**	Compound **4**
Empirical formula	C23 H17 N O4	C23 H17 N O4
Mr	371.39	371.38
T (K)	173(2)	173
Crystal system	Orthorhombic	Monoclinic
Space group	Pccn	P21/c
a (Å)	16.996(2)	10.5324(16)
b (Å)	13.8172(19)	17.783(3)
c (Å)	14.783(2)	9.2757(15)
α (°)	90	90
β (°)	90	93.650(3)
γ (°)	90	90
V (Å^3)	3471.7(8)	1733.8(5)
Z	8	4
D_c (g cm^{-3})	1.421	1.419
Crystal size	0.43 × 0.42 × 0.41	0.42 × 0.41 × 0.23
θ range for data collection (°)	1.90–27.05	1.94–27.05
Limiting indices (hkl)	$-21 \le h \le 21$; $-17 \le k \le 12$; $-18 \le l \le 13$	$-13 \le h \le 13$; $-22 \le k \le 22$; $-11 \le l \le 9$
Reflections collected	16,787	3764
Independent reflections (R_{int})	2820	2923
Good-of-fit on F^2	1.041	1.031
R_1/wR_2 $[I > 2\sigma(I)]$[a]	0.0391/0.0970	0.0440/0.1173
R_1/wR_2 (all data)[a]	0.0575/0.1089	0.0590/0.1293
Largest diff. peak (eÅ^{-1})	0.280/−0.203	0.743/−0.239

Protein-Binding Studies

Binding of compounds with bovine serum albumin (BSA) was studied from the fluorescence spectra recorded with an excitation at 280 nm and corresponding emission at 345 nm assignable to that of bovine serum albumin (BSA). The excitation and emission slit widths and scan rates were kept constant for all the experiments. Sample solutions were carefully degassed using pure nitrogen gas for 15 min using quartz cells with high-vacuum Teflon stopcocks. Stock solution of BSA was prepared in 50 mM phosphate buffer (pH 7.2) and stored in the dark at 4 °C for further use. Concentrated stock solutions of the complexes were prepared by dissolving them in DMSO: phosphate buffer (5:95) and diluted suitably with phosphate buffer to required concentrations. 2.5 mL of BSA solution (1 mM) was titrated by successive additions of a 5 mL stock solution of compounds (10^{-4} M) using a micropipette. Synchronous fluorescence spectra were also recorded using the same concentration of BSA and compounds as mentioned above with two different $\Delta\lambda$ (difference between the excitation and emission wavelengths of BSA) values such as 15 and 60 nm.

DNA Cleavage Studies

The DNA cleavage was studied by agarose gel electrophoresis experiment. The supercoiled pBR322 DNA was treated with the compounds, and the mixture was irradiated for 40 min with a UV lamp (365 nm, 10 W). The samples were analyzed by electrophoresis for 2.0 h at 80 V on a 1.0 % agarose gel in TBE (89 mM Tris–Borate acid, 2 mM EDTA, pH 8.3). The gel was stained with 1 mg/mL ethidium bromide and photographed on an Alpha Innotech IS-5500 fluorescence chemiluminescence and visible imaging system.

In Vitro Cytotoxicity Assay

Standard 3-(4,5-dimethylthiazole)-2,5-diphenyltetrazolium bromide (MTT) assay procedures were used. Cells were placed in 96-well microassay culture plates (1×10^4 cells per well) and grown overnight at 37 °C in a 5 % CO_2 incubator. Compounds tested were dissolved in DMSO and diluted with Roswell Park Memorial Institute 1640 (RPMI 1640) to the required concentrations prior to use. Control wells were prepared by the addition of culture medium

(100 μL). Wells containing culture medium without cells were used as blanks. The plates were incubated at 37 °C in a 5 % CO_2 incubator for 48 h. Upon completion of the incubation, stock MTT dye solution (20 μL, 5 mg mL^{-1}) was added to each well. After 4-h incubation, buffer (100 μL) containing dimethylformamide (50 %) and sodium dodecyl sulfate (20 %) was added to solubilize the MTT formazan. The optical density of each well was then measured on a microplate spectrophotometer at a wavelength of 490 nm. The IC_{50} values were determined by plotting the percentage viability versus concentration on a logarithmic graph and reading off the concentration at which 50 % of cells remain viable relative to the control. Each experiment was repeated at least three times to obtain the mean values. Four different tumor cell lines BEL-7402, HeLa, A549, and SK-BR-3 were investigated.

Comet Assay

DNA damage was investigated by means of comet assay. BEL-7402 cells in culture medium were incubated with 25 and 50 μM of complexes **3** and **4** for 24 h at 37 °C. The control cells were also incubated at the same time. The cells were harvested by a trypsinization process at 24 h. A total of 100 μL of 0.5 % normal agarose in PBS was dropped gently onto a fully frosted microslide, covered immediately with a coverslip, and then placed at 4 °C for 10 min. The coverslip was removed after the gel had set. 50 μL of the cell suspension (200 cells/μL) was mixed with 50 μL of 1 % low melting agarose preserved at 37 °C. A total of 100 μL of this mixture was applied quickly on top of the gel, coated over the microslide, covered immediately with a coverslip, and then placed at 4 °C for 10 min. The coverslip was again removed after the gel had set. A third coating of 50 μL of 0.5 % low melting agarose was placed on the gel and allowed to set at 4 °C for 15 min. After solidification of the agarose, the coverslips were removed and the slides were immersed in an ice-cold lysis solution (2.5 M NaCl, 100 mM EDTA, 10 mM Tris, 90 mM sodium sarcosinate, NaOH, pH 10, 1 % Triton X-100, and 10 % DMSO) and placed in a refrigerator at 4 °C for 2 h. All of the above operations were performed under low lighting conditions to avoid additional DNA damage. The slides, after removal from the lysis solution, were placed horizontally in an electrophoresis chamber. The reservoirs were filled with an electrophoresis buffer (300 mM NaOH, 1.2 mM EDTA) until the slides were just immersed in it, and the DNA was allowed to unwind for 30 min in electrophoresis solution. Then the electrophoresis was carried out at 25 V and 300 mA for 20 min. After electrophoresis, the slides were removed and washed thrice in a neutralization buffer (400 mM Tris, HCl, pH 7.5). Nuclear DNA was stained with 20 μL of EtBr (20 μg/mL) in the dark for 20 min. The slides were washed in chilled distilled water for 10 min to neutralize the excess alkali, air-dried, and scored for comets by fluorescence microscopy.

Apoptosis Assessment by AO/EB Staining

A monolayer of BEL-7402 cells was incubated in the absence and presence of the compounds at a concentration of 25 μM at 37 °C and 5 % CO_2 for 24 h. Then each cell culture was stained with AO/EB solution (100 μg mL^{-1} AO, 100 μg mL^{-1} EB) and observed by fluorescence microscopy. It is well known that AO can pass through cell membranes, but EB cannot. Under the fluorescence microscope, living cells appear green. Necrotic cells stain red but have a nuclear morphology which resemble viable cells. Apoptotic cells appear green, and morphological changes such as cell blebbing and formation of apoptotic bodies will be observed.

Cellular Uptake Study

Cells were placed in 24-well microassay culture plates (4×10^4 cells per well) and grown overnight at 37 °C in a 5 % CO_2 incubator. Compounds tested were then added to the wells. The plates were incubated at 37 °C in a 5 % CO_2 incubator for 48 h. Upon completion of the incubation, the wells were washed three times with PBS. After removing the culture medium, the cells were stained with 2-(4-amidinophenyl)-6-indolecarbamidine dihydrochloride (DAPI) and observed under fluorescence microscope.

Reactive Oxygen Species (ROS) Detection

BEL-7402 cells were seeded into six-well plates (Costar, Corning, Corning, NY, USA) at a density of 2×10^5 cells per well. The cells were cultured in RPMI 1640 supplemented with 10 % of FBS and incubated at 37 °C and 5 % CO_2. The medium was removed. Then new medium and 25 μM of compounds (the compounds were dissolved in DMSO and final DMSO concentration is 0.05 % v/v) were added and cultured for 24 h. The medium was again removed. The fluorescent dye 2′,7′-dichlorodihydrofluorescein diacetate (DCHF-DA) was added to cover the cells. The treated cells were then washed with cold PBS-EDTA twice. Fluorescence-activated cell was observed under fluorescence microscope.

Mitochondrial Membrane Potential Detection

BEL-7402 cells were treated for 24 h with the compounds in 12-well plates and were then washed three times with cold PBS. The cells were detached with trypsin–EDTA solution. Collected cells were incubated for 20 min with

1 μg/mL 5,5′,6,6′-tetrachloro- 1,1′,3,3′-tetraethylbenzimidazolcarbocyanine iodide (JC-1) in culture medium at 37 °C in the dark. The cells were immediately centrifuged to remove the supernatant. Cell pellets were suspended in PBS and then imaged by a fluorescence microscope.

Western Blot Analysis

BEL-7402 cells were seeded in 3.5-cm dishes for 24 h and incubated with compounds **3** and **4** (12.5 μM) in the presence of 10 % FBS. Then the cells were harvested in lysis buffer. After sonication, the samples were centrifuged for 20 min at 13,000×*g*. The protein concentration of the supernatant was determined by BCA assay. Sodium dodecyl sulfate–polyacrylamide gel electrophoresis was done loading equal amount of proteins per lane. Gels were then transferred to poly (vinylidene difluoride) membranes (Millipore) and blocked with 5 % non-fat milk in TBST buffer for 1 h. Then the membranes were incubated with primary antibodies at 1:5000 dilutions in 5 % non-fat milk overnight at 4 °C and washed four times with TBST for a total of 30 min; after which the secondary antibodies were conjugated with horseradish peroxidase at 1:5000 dilution for 1 h at room temperature and then washed four times with TBST. The blots were visualized with the Amersham ECL Plus western blotting detection reagents according to the manufacturer's instructions. To assess the presence of comparable amount of proteins in each lane, the membranes were stripped finally to detect the β-actin.

Results and Discussion

Synthesis, Characterization, and Structure

Compounds **3** and **4** were prepared by the domino oxidant reaction of binaphthol **2** in the presence of $CuCl_2$–ethanolamine complex. Methanol was used as a nucleophile to provide 13*c*-alkoxy group of dibenzoxanthene. The compounds were characterized by ^{1}H NMR, electrospray mass spectroscopies, and elemental analysis. The molecular structures of compounds **3** and **4** were further authenticated by single-crystal X-ray diffraction analysis. The crystal data for two compounds are listed in Table 1, and the selected bond lengths and bond angles are listed in Table 2. The ORTEP drawing of compounds **3** and **4** with atomic numbering scheme is depicted in Fig. 1. For compound **3**, 2-position carbon of compound **2** was oxidized into carboxyl and a methoxyl was added to carbon 1. Five rings of the product are almost coplanar. However, for compound **4**, 2′-position carbon of compound **2** was oxidized into carboxyl and a methoxyl was also added to carbon 1′.

Crystallographic data (excluding structure factors) for the structures reported in this work have been deposited in the Cambridge Crystallographic Data Centre as supplementary publication. No. CCDC- 950468 for compound **3** and No. CCDC-951502 for compound **4**. Copies of the data can be obtained free of charge on application via www.ccdc.cam.ac.uk/data_request/cif or e-mail (deposit@ccdc.cam.ac.uk).

DNA-Binding Studies

Electronic Absorption Spectra

The electronic absorption titration was performed with increasing concentrations of calf thymus DNA (CT DNA). With increasing the amounts of CT DNA, the changes in absorbance at 360 nm for compound **3** and 330 nm for compound **4** are observed (Fig. 2). The hypochromism is 45.83 % with red shift of 3 nm and 26.32 % with red shift of 2 nm for compounds **3** and **4**, respectively.

Table 2 Selected bond length (Å) and angle (°) for compounds **3** and **4**

Compound **3**			
O1–C8	1.3794	O2–C21	1.4245
O1–C9	1.3698	O3–C16	1.2115
O2–C17	1.4540	O4–C22	1.2279
C8–O1–C9	118.52	O2–C17–C19	112.51
C17–O2–C21	114.75	O2–C17–C16	100.83
C22–N1–C23	120.64	O2–C17–C18	110.12
O1–C8–C19	124.67	C18–C17–C19	111.43
O1–C8–C7	112.35	C16–C17–C19	115.06
O1–C9–C10	116.17	C16–C17–C18	106.26
C14–C15–C16	118.01	C9–C18–C17	122.70
C16–C15–C22	123.02	C8–C19–C20	117.49
O3–C16–C17	122.94	C8–C19–C17	119.88
C15–C16–C17	113.52	C17–C19–C20	122.57
Compound **4**			
O1–C8	1.3764(19)	O3–C21	1.414(2)
O1–C20	1.3741(19)	O4–C22	1.236(2)
O2–C1	1.209(2)	N1–C22	1.332(2)
O3–C10	1.4584(19)	N1–C23	1.458(2)
C8–O1–C20	119.34(12)	O3–C10–C1	100.80(11)
C10–O3–C21	114.21(12)	O3–C10–C9	109.09(13)
C22–N1–C23	120.88(14)	O3–C10–C11	112.38(13)
O2–C1–C2	122.10(15)	C1–C10–C9	106.71(13)
O2–C1–C10	123.99(16)	C1–C10–C11	115.45(14)
C2–C1–C10	113.88(15)	C9–C10–C11	111.70(12)
C1–C2–C3	119.95(16)	C12–C11–C20	118.30(14)
O1–C8–C7	116.15(13)	C11–C12–C13	123.75(15)
O1–C8–C9	121.55(14)	C11–C12–C17	118.72(14)

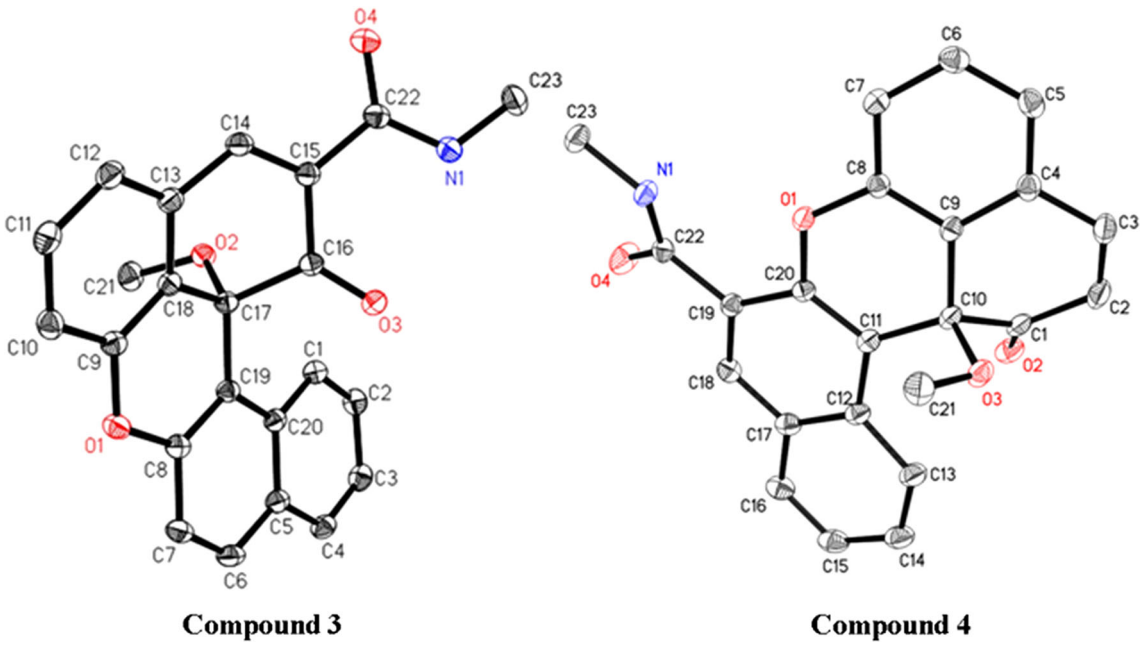

Fig. 1 ORTEP drawing of compounds **3** and **4**

Hypochromism is caused by the strong interaction between compounds and CT DNA base pairs (Ramakrishnan et al. 2011). These characteristics indicate that two compounds interact with DNA most likely through a mode that involves a stacking interaction between the aromatic chromophore and the base pairs of DNA. To compare quantitatively the binding strength of two compounds, the intrinsic constants K_b were determined from absorption titration data. The values of K_b are 2.51 ($\pm$0.09) $\times$ 10^3 for compound **3** and 4.55 ($\pm$0.10) $\times$ 10^3 for compound **4**, respectively. These values are of the same order as that of dibenzoxanthene compounds (Wang et al. 2012).

Viscosity Measurements

In order to understand the DNA-binding mode of two compounds **3** and **4**, viscosity measurements were carried out. A classical intercalation of a ligand into DNA is known to cause a significant increase in the viscosity of a DNA solution due to an increase in the separation of the base pairs at the intercalation site and, hence, an increase in the overall DNA molecular length (Waring 1965). The effects of compounds **3** and **4** on the viscosity of rod-like DNA are shown in Fig. 3. As seen in Fig. 3, we found that upon increasing the amounts of compounds **3** and **4** (the ratios of [compound]/[DNA] range from 0.00 to 0.16), the relative viscosity of CT DNA solution increases steadily. The ability to increase the viscosity of DNA is **3** > **4**. These results suggest that two compounds can bind to CT DNA through intercalation mode.

Fluorescence Studies

At room temperature, compounds **3** and **4** exhibit luminescence in Tris buffer with a maximum at 508 nm for **3** and 510 nm for **4**. As shown in Fig. 4, the luminescence intensity increases with increasing concentrations of CT DNA. When the ratio of [DNA]/[compound] reached a saturated value, the emission intensities of compounds **3** and **4** increased 2.34 and 6.28 times than the original. Compound **4** causes larger increase in emission intensity than compound **3** under the same conditions. This implied that the compounds can intercalate into CT DNA base pairs and be protected by DNA efficiently, since the hydrophobic environment inside the DNA helix reduces the accessibility of water to the compound and the compound mobility is restricted at the binding site, leading to the decrease of vibrational modes of relaxation.

Protein-Binding Studies

Fluorescence spectroscopy has proved to be an efficient tool in the investigation of interaction of compounds with BSA. Fluorescence of BSA arises due to the presence of fluorophores like tryptophan, tyrosine, and phenylalanine, and quenching is usually induced by a variety of molecular interactions such as excited-state reactions, molecular rearrangements, energy transfer, etc. (Raja et al. 2013). Therefore, BSA fluorescence quenching experiments in the presence of compounds were also investigated. The results are depicted in Fig. 5. An examination of the spectrum

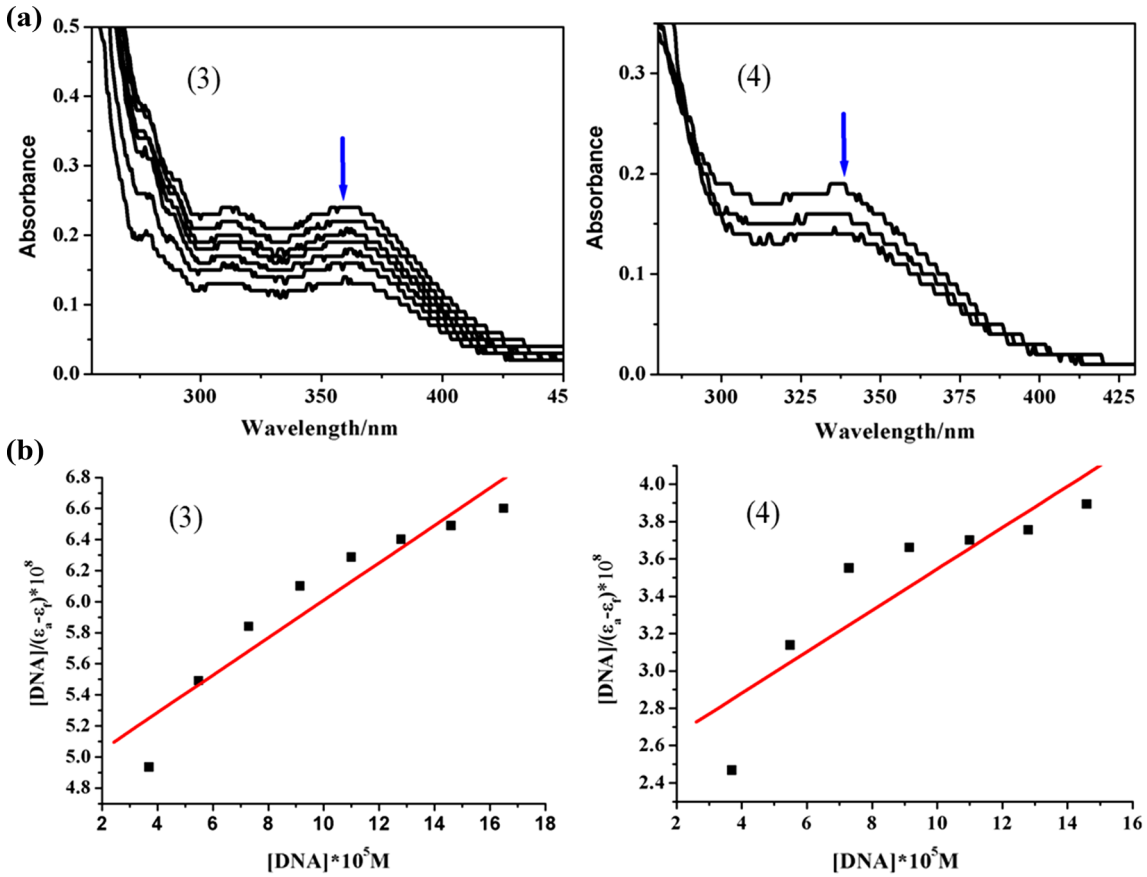

Fig. 2 **a** Absorption spectra of compounds **3** and **4** in Tris–HCl buffer upon addition of CT DNA. *Arrows* show the absorbance change upon increase of DNA concentration. **b** DNA-binding constants by $[DNA]/(\varepsilon_a - \varepsilon_f)$ versus [DNA] for the titration of DNA with two compounds

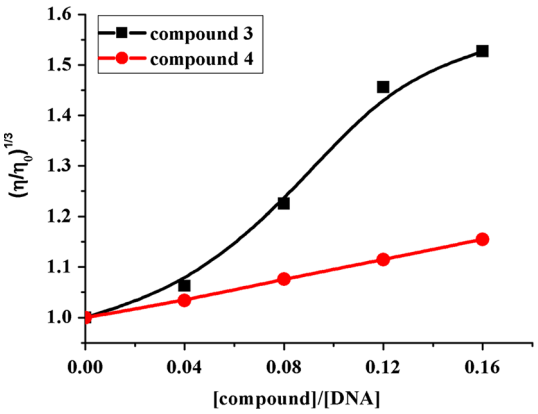

Fig. 3 Relative viscosity changes of CT DNA solutions (250 μM) in the presence of different concentrations of compounds **3** and **4**

showed a noteworthy decrease in fluorescence intensity at 344 nm, 40.1 % for compound **3** and 29.4 % for compound **4**. The fluorescence quenching is described by Stern–Volmer relation: $I_0/I = 1 + K_{SV}[Q]$, where I_0 and I are the fluorescence intensities of the fluorophore in the absence and presence of quencher, respectively; K_{SV} is the Stern–Volmer quenching constant; and $[Q]$ is the quencher concentration. K_{SV} values obtained from the plot of I_0/I versus $[Q]$ were found to be 1.165×10^5 for compound **3** and 1.060×10^5 for compound **4**. The binding ability follows the order of **3** > **4**. The calculated values for the two test compounds exhibit their strong protein-binding ability.

UV–visible absorption measurement is a simple method to explore the structural changes and is useful to distinguish whether the type of quenching exists is static or dynamic. Dynamic quenching only affects the excited states of the fluorophore, and there are no changes in the absorption spectra (Paitandi et al. 2014; Sathyadevi et al. 2012). The absorption spectra of BSA in the absence and presence of two compounds at different concentrations were studied. Figure 6 shows that upon increasing the concentration of two compounds, absorption intensities of BSA decreased regularly, due to the adsorption of BSA on the surface of the compounds **3** and **4**.

Photoinduced Cleavage of pBR322 DNA

To explore the DNA cleavage abilities of compounds **3** and **4**, the gel electrophoresis experiments were performed

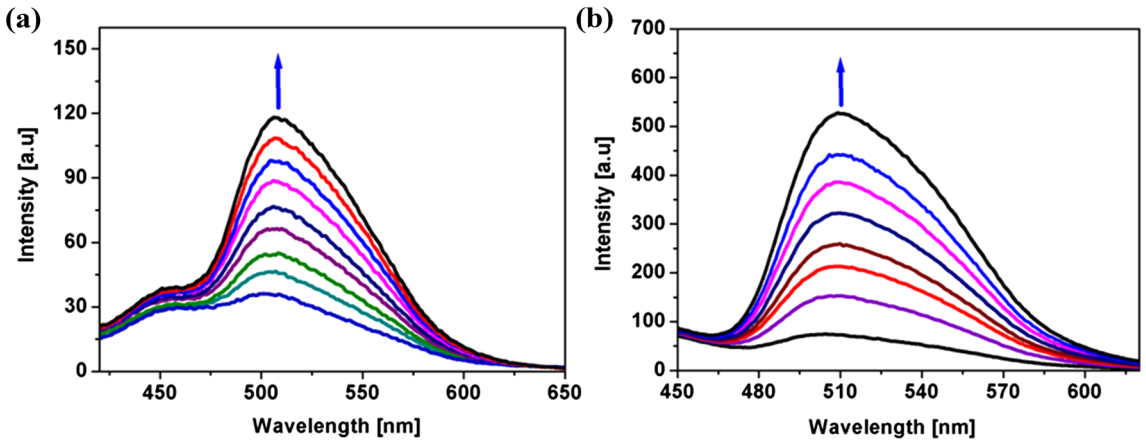

Fig. 4 Emission spectra of compounds **3** (**a**) and **4** (**b**) in Tris–HCl buffer in the absence and presence of CT DNA. *Arrow* shows the intensity change upon increasing DNA concentrations

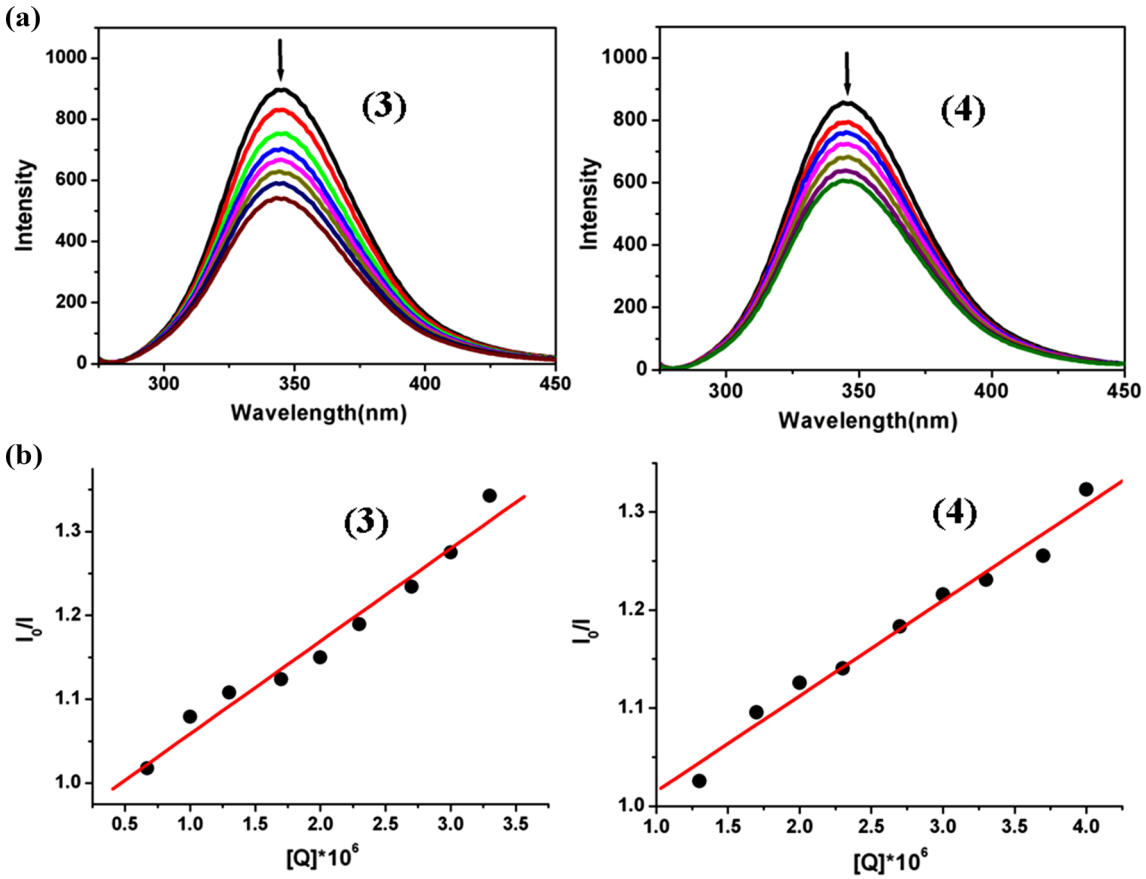

Fig. 5 **a** Emission spectra of BSA upon addition of compounds **3** and **4**. **b** The K_{SV} values obtained from the plot of I_0/I versus [Q]

upon irradiation. When circular plasmid DNA is subjected to electrophoresis, relatively fast migration will be observed for the intact supercoiled form (Form I). If scission occurs on one strand (nicking), the supercoiled form will relax to generate a slower moving open circular form (Form II) (Barton and Raphael 1984). Figure 7 shows gel electrophoresis separation of pBR322 DNA after incubation with different concentrations of compounds **3** and **4** upon irradiation at 356 nm for 45 min. In the control (DNA alone) or incubation with compounds in darkness, no obvious DNA cleavage was found. When pBR322 DNA was treated with different concentrations of compounds,

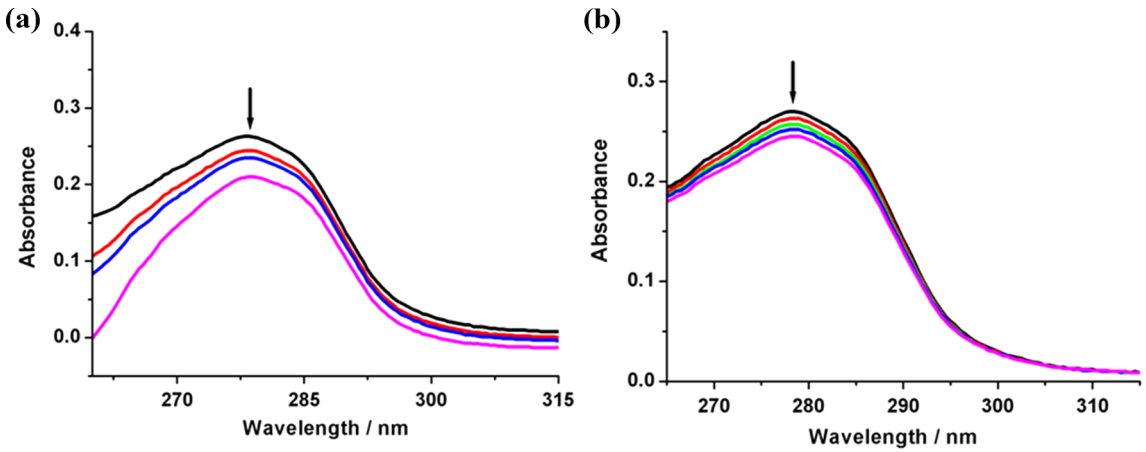

Fig. 6 The absorption spectra of BSA upon addition of compound **3** (**a**) and compound **4** (**b**). *Arrows* show the absorbance of BSA change upon increase of compound concentrations

the Form II was observed. Because the experiment was observed upon irradiation, the DNA cleavage induced by two compounds is caused by oxidation.

Cytotoxicity Assay In Vitro

The cytotoxic activity of compounds is closely related to their structures. The antiproliferative effect of the compounds on BEL-7402, HeLa, A549, and SK-BR-3 cells was assayed using MTT method. The IC_{50} values are listed in Table 3. Comparing the IC_{50} values of compounds **3** and **4**, two compounds have different cytotoxic activities. Compound **4** shows higher cytotoxic activity in BEL-7402 and HeLa cells. This may be caused by the different structures of the two compounds. Unexpectedly, two compounds show low cytotoxic activity toward SK-BR-3 cells.

Table 3 The IC_{50} values for compounds **3** and **4**

Compounds	IC_{50} (μM)			
	BEL-7402	HeLa	A549	SK-BR-3
3	19.3 ± 1.5	31.5 ± 2.5	58.4 ± 2.8	>100
4	9.59 ± 0.8	13.4 ± 2.2	96.3 ± 4.5	>100

Compounds Induced to Cellular DNA Damage

The comet assay, or alkaline single-cell gel electrophoresis, is a rapid, simple, and sensitive technique for measuring and analyzing DNA breakage in individual cells (Collins et al. 2008; Wasson et al. 2008). And therefore, it is an ideal biomarker for the identification of agents with anticancer potentials. In this paper, we used comet assay to determine whether compounds **3** and **4** could induce cellular DNA damage of BEL-7402 cells. As shown in Fig. 8, the nuclei (the stained circles) from controls essentially remain intact with almost no visible comet tail (Fig. 8a). However, the nuclei from compound-treated BEL-7402 cells exhibited not only a shrunken morphology but also a prominent comet tail (Fig. 8b–e). After normalization against control cells, the comet tail of compound-treated cells significantly increased in a close-dependent manner. The results of comet assays in BEL-7402 cancer cells indicated that compounds **3** and **4** are capable of eliciting DNA-damaging effects.

Apoptosis Studies

Apoptosis induced by compounds is one of the considerations in drug development. The apoptotic cells usually have apoptotic features such as nuclear shrinkage and

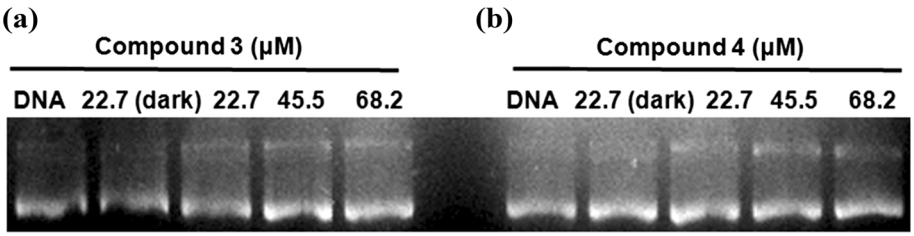

Fig. 7 Photoactivated cleavage of pBR322 DNA induced by different concentrations of compounds **3** (**a**) and **4** (**b**) upon irradiation at 365 nm for 40 min

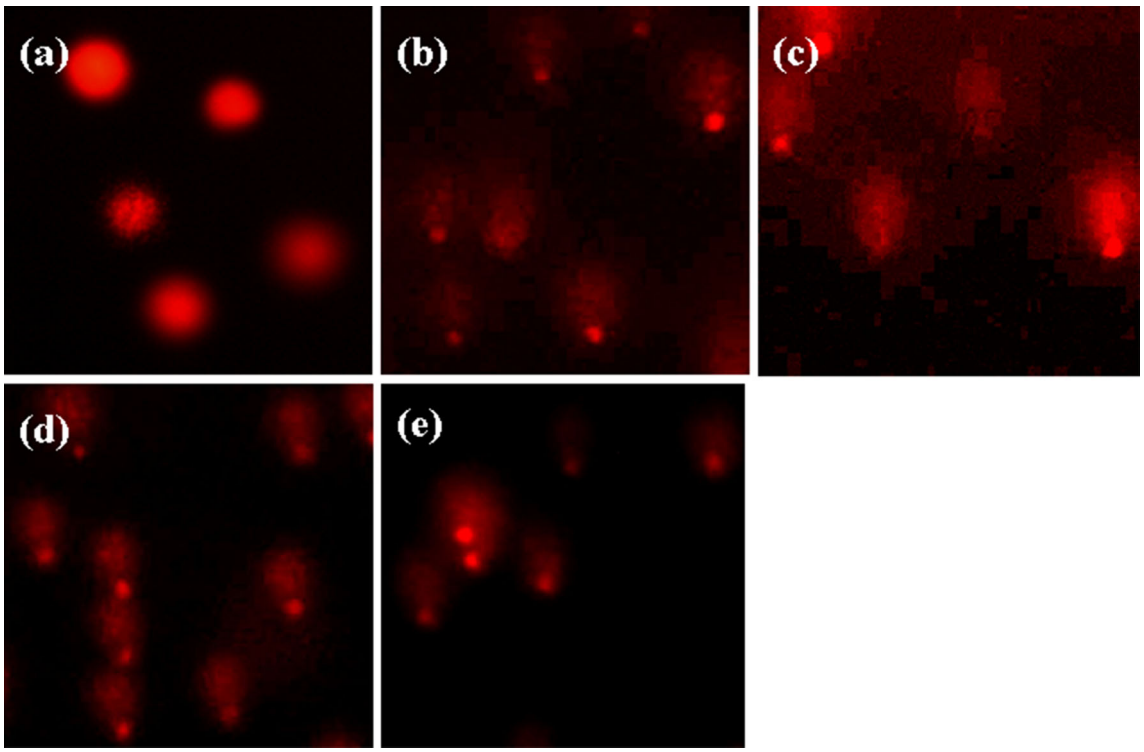

Fig. 8 Comet assay of EB-stained BEL-7402. **a** Control, **b** 25 μM of compound **3**, **c** 50 μM of compound **3**, **d** 25 μM of compound **4**, and **e** 50 μM of compound **4**

chromatin condensation (Liu et al. 2011). Apoptosis assay was carried out with AO and EB staining method. To determine whether the cell death is associated with apoptosis, BEL-7402 cells were exposed to compounds **3** and **4** for 24 h and observed under fluorescence microscope. As shown in Fig. 9, in the control, the living cells were stained bright green in spots (Fig. 9a). After the treatment of BEL-7402 cells with the compounds for 24 h, green apoptotic cells containing apoptotic bodies stained by acridine orange were found (Fig. 9b, c). These results suggested that compounds **3** and **4** can induce apoptosis of BEL-7402 cells.

Cellular Uptake Study

The uptake of compounds **3** and **4** by BEL-7402 cells was carried out. Compounds **3** and **4** at 12.5 μM were added to the well (4×10^3 cells per well). After the treatment for 24 h, the cells were stained with DAPI and observed under fluorescence microscope. As shown in Fig. 10, the blue channel shows DAPI-stained nuclei with an excitation wavelength of 340 nm, the green channel displays the luminescence of compounds **3** and **4** with an excitation wavelength of 310 nm, and the overlay represents cellular association of compounds **3** and **4**. The complete overlay between blue and green suggests that the compounds can be successfully taken up by BEL-7402 cells.

Measurement of Intracellular ROS Levels

Many potential anticancer and chemopreventive agents induce cell apoptosis through intracellular ROS generation. There are massive literatures to report that the growth inhibitory effect of compounds is accompanied by an increase of reactive oxygen species (Watson et al. 2008, 2010). To investigate whether the compounds can enhance the ROS levels, 2′,7′-dichlorodihydrofluorescein diacetate (DCHF-DA) was used as a fluorescent probe to detect ROS change in BEL-7402 cells. DCHF-DA is cleaved by intracellular esterases into its non-fluorescent form (DCHF). The DCHF is oxidized by intracellular free radicals to produce a fluorescent product dichlorofluorescein (DCF). As shown in Fig. 11, in the control (a), no fluorescence image is found. After BEL-7402 cells were exposed to 25 μM of compounds **3** (c) and **4** (d) for 24 h, the fluorescence images are observed. Moreover, it is also found that the fluorescence intensity of compound **3** is larger than that of compound **4**. These results suggest that compounds **3** and **4** can effectively enhance the intracellular ROS levels of BEL-7402 cells.

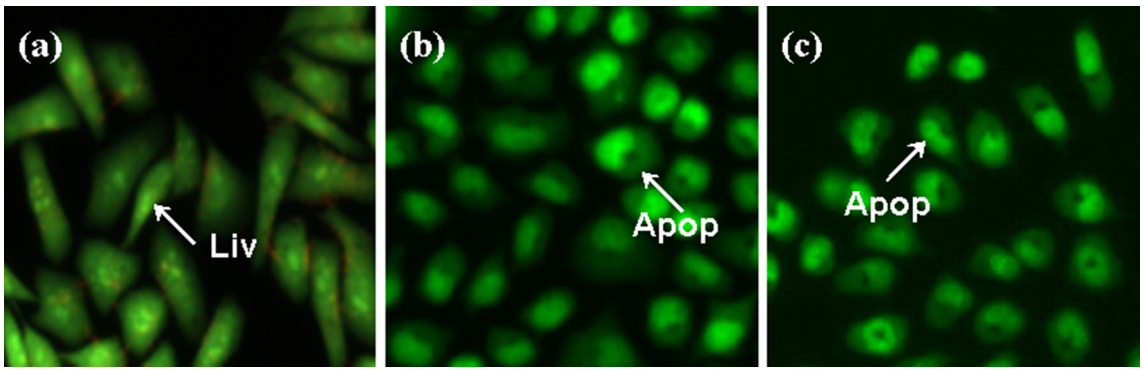

Fig. 9 AO/EB staining of BEL7402 cells. **a** Control cells and **b** cells' exposure to 25 μM compound **3** and **c** compound **4**; Liv stands for live cell and Apop for apoptotic cell

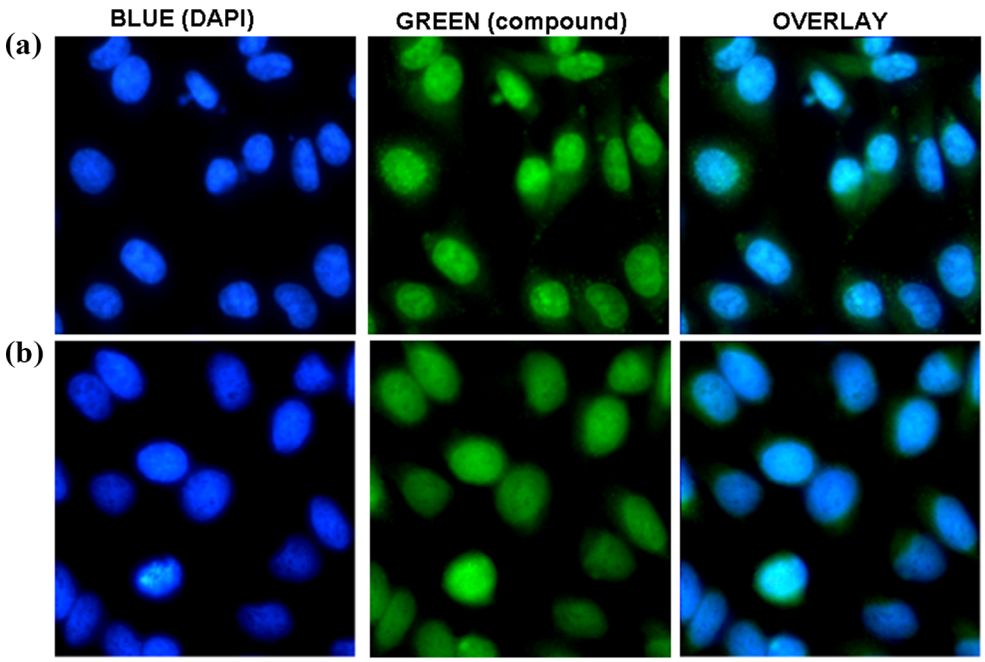

Fig. 10 Images of BEL-7402 cells' exposure to 12.5 μM of compounds **3** (**a**) and **4** (**b**) stained with DAPI at 37 °C for 24 h

Mitochondrial Membrane Potential Assay

Mitochondrial membrane plays a vital role in apoptosis triggered by chemical reagent. Chemical-induced apoptosis mediated by the mitochondrial/apoptotic cascades is often associated with the collapse of the mitochondrial membrane potential as a result of leakage of pro-apoptotic factors (Li et al. 2014). Mitochondrial dysfunction was determined using fluorescence microscopy after staining live cells with the cationic dye JC-1. As seen in Fig. 12a, JC-1 exhibits red fluorescence in the control corresponding to high mitochondrial membrane potential. After BEL-7402 cells were exposed to 25 μM of compounds **3** and **4** for 24 h, a significant increase of the green fluorescent is observed (Fig. 12c, d). The changes from red to green fluorescence suggest that compounds **3** and **4** induce the decrease of mitochondrial membrane potential.

Western Blot Analysis

Caspases are known to mediate the apoptotic pathway (Thornberry and Lazebnik 1998). To clarify the mechanism of apoptosis induced by compounds **3** and **4**, activation of caspase-3 and caspase-7 was assayed by western blot analysis. The results are shown in Fig. 13; after the treatment of caspase-3 and caspase-7 with two compounds, the levels of caspase-3 were diminished, whereas those of caspase-7 were increased. Bcl-2 family proteins play critical roles in the regulation of apoptosis via the control of mitochondrial membrane (Cory et al. 2003). It was

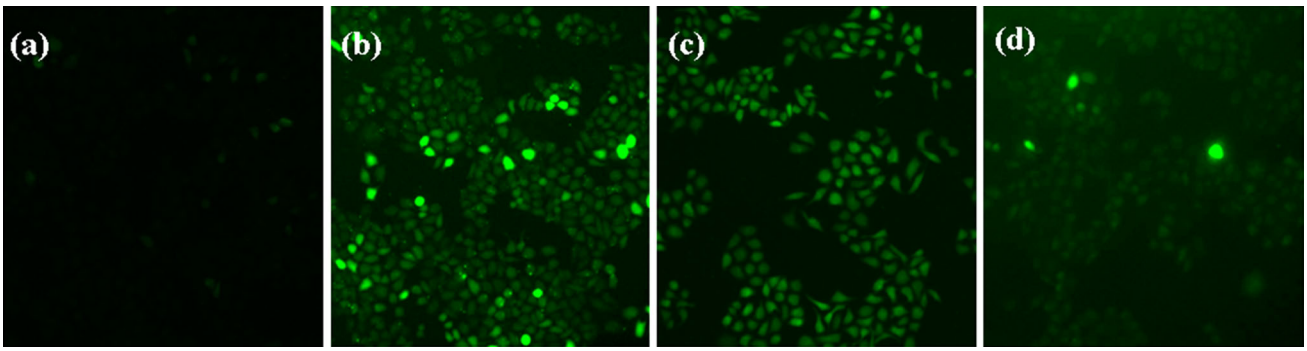

Fig. 11 Intracellular ROS detected in BEL7402 cells. **a** Control cells, **b** Rosup, **c** 25 μM of compound **3**, and **d** 25 μM of compound **4**. Rosup was used as a positive control

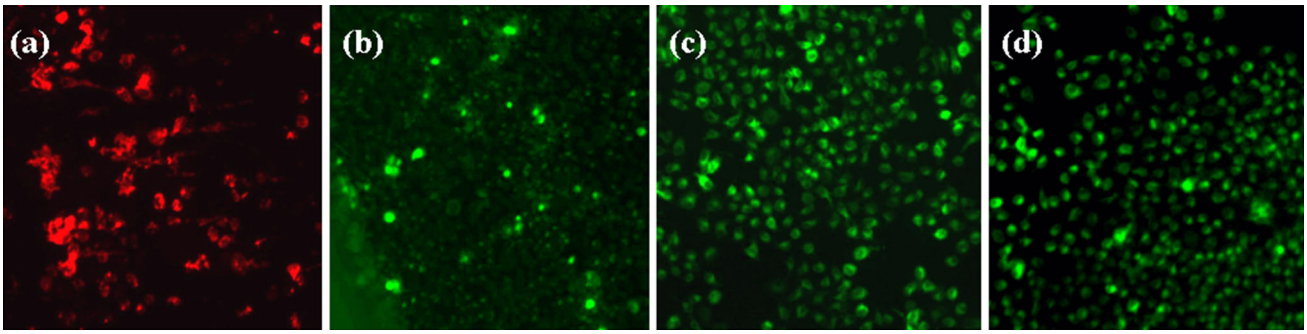

Fig. 12 Assay of BEL7402 cells mitochondrial membrane potential with JC-1 as a fluorescence probe staining method. **a** Control cells, **b** cccp, and **c** exposure to 25 μM of compound **3** and **d** compound **4**. cccp was used as a positive control

determined whether two compounds can induce changes in the levels of the Bcl-2 family proteins. On the treatment of anti-apoptotic protein Bcl-2 with 12.5 μM of compounds **3** and **4**, the down-regulation of the expression levels of Bcl-2 was observed. On the treatment of pro-apoptotic protein Bax with two compounds, the expression levels were up-regulated. These results indicate that compounds **3** and **4** induce apoptosis in Bel-7402 cells through activation of caspase-3 and caspase-7, down-regulation of Bcl-2, and up-regulation of Bax.

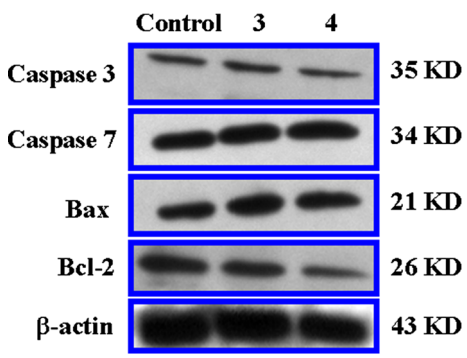

Fig. 13 Western blot analysis of caspase-3, caspase-7, Bcl-2, and Bax in BEL-7402 cells' exposure to compounds **3** and **4** for 24 h; b-actin was used as an internal control

Conclusion

Two dibenzoxanthene isomers **3** and **4** have been synthesized and characterized by X-ray crystals. The DNA-binding behaviors show that two compounds interact with CT DNA by intercalative mode. Further interaction with protein (BSA) has been investigated by UV–vis and fluorescence spectroscopy. The results suggest that compounds exhibit strong BSA-binding abilities. Compounds **3** and **4** can induce pBR322 DNA cleavage under photoactive condition. Comet assay demonstrated that two compounds can induce cellular DNA damage. The cytotoxicity assay indicates that compound **4** exhibits higher anticancer activity than compound **3** against BEL-7402 and HeLa cell lines. The AO/EB nuclear staining assay reveals that the compounds can induce apoptosis of BEL-7402 cells. The cellular uptake shows that these compounds can enter into the cytoplasm and accumulate in the nuclei. Additionally, compounds **3** and **4** can enhance the level of intracellular ROS. Two compounds can induce a decrease of mitochondrial membrane potential. Western blot analysis shows that two compounds can activate caspase-3 and caspase-7, downregulate the level of anti-apoptotic Bcl-2, and upregulate the levels of pro-apoptotic Bax. These results

display that the compounds induce apoptosis of BEL-7402 cells through mitochondrial dysfunction pathway.

Acknowledgments This work was supported by the Priority Academic Program Development of Guangdong Higher Education Institutions (2013LYM0047), the High-Level Personnel Project in 2013 of Guangdong Province, and the Joint Nature Science Fund of the Department of Science and Technology and the First Affiliated Hospital of Guangdong Pharmaceutical University (No. GYFYLH201315).

References

Ahmad M, King TA, Ko DK, Cha BH, Lee J (2002) Performance and photostability of xanthene and pyrromethene laser dyes in sol-gel phases. J Phys D Appl Phys 35:1473–1476

Barton JK, Raphael AL (1984) Photoactivated stereospecific cleavage of double-helical DNA by cobalt (III) complexes. J Am Chem Soc 106:2466–2468

Bekaert A, Andrieux J, Plat M (1992) New total synthesis of bikaverin. Tetrahedron Lett 33:2805–2806

Chaires JB, Dattagupta N, Crothers DM (1982) Studies on interaction of anthracycline antibiotics and deoxyribonucleic acid: equilibrium binding studies on the interaction of daunomycin with deoxyribonucleic acid. Biochemistry 21:3933–3940

Cohen G, Eisenberg H (1969) Viscosity and sedimentation study of sonicated DNA-proflavine complexes. Biopolymers 8:45–55

Collins AR, Oscoz AA, Brunborg G, Gaivaõ I, Giovannelli L, Kruszewski M, Smith CC, Stetina R (2008) The comet assay: topical issues. Mutagenesis 23:143–151

Cory S, Huang DC, Adams JM (2003) The Bcl-2 family: roles in cell survival and oncogenesis. Oncogene 22:8590–8607

Gong K, Fang D, Wang HL, Zhou XL, Liu ZL (2009) The one-pot synthesis of 14-alkyl- or aryl-14H-dibenzo[a, j]xanthenes catalyzed by task-specific ionic liquid. Dyes Pigm 80:30–33

Hafez HN, Hegab MI, Ahmed-Farag IS, El-Gazzar ABA (2008) A facile regioselective synthesis of novel spiro-thioxanthene and spiro-xanthene-9',2 -[1,3,4]thiadiazole derivatives as potential analgesic and anti-inflammatory agents. Bioorg Med Chem Lett 18:4538–4543

Hecht SM (2000) Bleomycin: new perspectives on the mechanism of action. J Nat Prod 63:158–168

Hideo T, Teruomi J (1981) (Sankyo Co.) Japan Patent 56005480

Ion RM (1997) The photodynamic therapy of cancer—a photosensitization or a photocatalytic process. Prog Catal 2:55–76

Jha A, Beal J (2004) Convenient synthesis of 12H-benzo[a]xanthenes from 2-tetralone. Tetrahedron Lett 45:8999–9001

Kelly JM, Murphy MJ, Mcconnell DJ, Ohuigin CA (1985) 5,10,15,20 -tetrakis(N-methylpyridinium-4-yl)porphyrin and its zinc complex with DNA using fluorescence spectroscopy and topoisomerisation. Nucleic Acids Res 13:167–184

Knight DW, Little PB (2001) The first efficient method for the intramolecular trapping of benzynes by phenols: a new approach to xanthenes. J Chem Soc Perkin Trans 15:1771–1777

Knight CG, Stephens T (1989) Xanthene-dye-labelled phosphatidylethanolamines as probes of interfacial pH. studies in phospholipid vesicles. Biochem J 258:683–687

Lambert RW, Martin JA, Merrett JH, Parkes KEB, Thomas GJ (1997) CT Int. Appl. WO9706178

Li W, Jiang GB, Yao JH, Wang XZ, Wang J, Han BJ, Xie YY, Lin GJ, Huang HL, Liu YJ (2014) Ruthenium(II) complexes: DNA-binding, cytotoxicity, apoptosis, cellular localization, cell cycle arrest, reactive oxygen species, mitochondrial membrane potential and western blot analysis. J Photochem Photobiol B 140:94–104

Liu YJ, Liang ZH, Li ZZ, Yao JH, Huang HL (2011) Cellular uptake, cytotoxicity, apoptosis, antioxidant activity and DNA binding of polypyridyl ruthenium(II) complexes. J Organomet Chem 696:2728–2735

Menchen SM, Benson SC, Lam JYL, Zhen W, Sun D, Rosenblum BB, Khan SH, Taing M (2003) U.S. Patent 6583168

Nandi GC, Samai S, Kumar R, Singh MS (2009) An efficient one-pot synthesis of tetrahydrobenzo[a]xanthene-11-one and diazabenzo[a]anthracene-9,11-dione derivatives under solvent free condition. Tetrahedron 65:7129–7134

Ohishi T, Kojima T, Matsuoka T, Shiro M, Kotsuko H (2001) High-yielding TfOH-catalyzed condensation of phenols with aromatic aldehydes at high pressure. A model synthesis of the benzylidene biphenol key skeleton of blepharismins. Tetrahedron Lett 42:2493–2496

Paitandi RP, Gupta RK, Singh RS, Sharma G, Koch B, Pandey DS (2014) Interaction of ferrocene appended Ru(II), Rh(III) and Ir(III) dipyrrinato complexes with DNA/protein, molecular docking and antitumor activity. Eur J Med Chem 84:17–29

Poupelin JP, Saint-Ruf G, Foussard-Blanpin O, Marcisse G, Uchida-Earnauf G, Lacroix R (1978) 3,3,6,6-Tetramethyl-9-phenyl-3,4,5,6-tetrahydro-9H-xanthene-1,8 (2H,7H) -dione. Eur J Med Chem 13:67–71

Raja DS, Ramachandran E, Bhuvanesh NSP, Natarajan K (2013) Synthesis, structure and *in vitro* pharmacological evaluation of a novel 2-oxo-1,2-dihydro quinoline-3-carbaldehyde (2′-methylbenzoyl) hydrazone bridged copper(II) coordination polymer. Eur J Med Chem 64:148–159

Ramakrishnan S, Shakthipriya D, Suresh E, Periasamy VS, Akbarsha MA, Palaniandavar M (2011) Ternary dinuclear copper(II) complexes of a hydroxybenzamide ligand with diimine coligands: the 5,6-dmp ligand enhances DNA binding and cleavage and induces apoptosis. Inorg Chem 50:6458–6471

Reichmann ME, Rice SA, Thomas CA, Doty P (1954) A further examination of the molecular weight and size of deoxypentose nucleic acid. J Am Chem Soc 76:3047–3053

Saint-Ruf G, Hieu HT, Poupelin JP (1975) The effect of dibenzoxanthenes on the paralyzing action of zoxazolamine. Naturwissenschaften 62:584–585

Sathyadevi P, Krishnamoorthy P, Bhuvanesh NSP, Kalaiselvi P, Padma VV, Dharmaraj N (2012) Organometallic ruthenium(II) complexes: synthesis, structure and influence of substitution at azomethine carbon towards DNA/BSA binding, radical scavenging and cytotoxicity. Eur J Med Chem 55:420–431

Satyanarayana S, Dabrowiak JC, Chaires JB (1993) Tris(phenanthroline) ruthenium(II) enantiomer interactions with DNA: mode and specificity of binding. Biochemistry 32:2573–2584

Sheldrick GM (1996) SADABS, program for empirical absorption correction of area detector data. University of Göttingen, Göttingen

Sheldrick GM (1997) SHELXL-97, program for crystal structure refinement. University of Göttingen, Göttingen

Thornberry NA, Lazebnik Y (1998) Requirement for MAPK activation for normal mitotic progression in xenopus egg extracts. Science 281:1312–1315

Wang XZ, Pang JY, Wang B, Xu ZL (2005) Study on cross-coupling reactions of substituted 2-naphthols promosted by copper (II)-amine complex. Chin J Org Chem 25:859–861

Wang XZ, Yang BY, Lin GJ, Xie YY, Huang HL, Liu YJ (2012) Cytotoxicity, cell cycle arrest, antioxidant activity and interaction of dibenzoxanthenes derivatives with DNA. DNA Cell Biol 31:1468–1474

Wang XZ, Xie YY, Yao JH, Lin GJ, Huang HL, Liu YJ (2013) Synthesis, DNA-binding and antioxidant activity studies of naphthoxazole compounds. Inorg Chem Commun 32:82–88

Wang XZ, Jiang GB, Xie YY, Liu YJ (2014) Synthesis, molecular structure, DNA interaction and antioxidant activity of novel naphthoxazole compound. Spectrochim Acta A 118:448–453

Waring MJ (1965) Complex formation between ethidium bromide and nucleic acids. J Mol Biol 13:269–274

Wasson GR, McKelvey-Martin VJ, Downes CS (2008) The use of the comet assay in the study of human nutrition and cancer. Mutagenesis 23:153–162

Watson JL, Hill R, Lee PW, Giacomantonio CA, Hoskin DW (2008) Curcumin induces apoptosis in HCT-116 human colon cancer cells in a p21-independent manner. Exp Mol Pathol 84:230–233

Watson JL, Hill R, Yaffe PB, Greenshields A, Walsh M, Lee PW, Giacomantonio CA, Hoskin DW (2010) Curcumin causes superoxide anion production and p53-independent apoptosis in human colon cancer cells. Cancer Lett 297:1–8

Wolf A, Shimer GH, Meehan T (1987) Polycyclic aromatic hydrocarbons physically intercalate into duplex regions of denatured DNA. Biochemistry 26:6392–6396

Zuber G, Quada JC Jr, Hecht SM (1998) Sequence selective cleavage of a DNA octanucleotide by chlorinated bithiazoles and bleomycins. J Am Chem Soc 120:9368–9369